© 2018 IJSRSET | Volume 4 | Issue 4 | Print ISSN: 2395-1990 | Online ISSN : 2394-4099
Themed Section : Engineering and Technology

Settled Graph Cut for Automatic Segmentation of High-recurrence Ultrasound Images of the Mouse Embryo

M. M. Raghavendra, P. Jyoshna, R. Suma, N. Chola Raju, V. Rajesh
ECE, JNTUA, Kurnool, Andhra Pradesh, India

ABSTRACT

We propose a completely programmed division method Uterus called settled diagram cut (NGC) to fragment pictures (2D or 3D) that contain numerous articles with a settled structure. Contrasted with other diagram cut-based techniques produced for different locales, our technique can function admirably for settled articles without requiring manual determination of introductory seeds, regardless of whether diverse items have 1 mm comparative power circulations and some protest limits are missing. Promising outcomes were acquired for isolating the brain (a) (b) (c) ventricles (BVs), the head, and the uterus locale in the mouse- developing life head pictures acquired utilizing high-recurrence ultrasound.

Keywords : NGC, HFU, MRI, 3D information securing, ASM

I. INTRODUCTION

WITH the broad information now accessible identified with the mouse genome, a large group of transgenic mice can be made with hereditary transformations that will be deadly in utero. Concentrate how these changes show themselves amid embryonic advancement as far as morphology and capacity, in a perfect world in 3D, will require constant imaging modalities and robotized picture preparing apparatuses [1]. Attractive reverberation imaging (MRI) and high-recurrence ultrasound (HFU) have turned into the most widely recognized imaging modalities for in vivo imaging of the creating mouse developing life [2][3]. Both imaging modalities are equipped for envisioning gross morphological deformities of mutant developing lives, in spite of the fact that the physical properties identified with picture differentiate vary. In spite of the fact that MRI can furnish solid tissue appear differently in relation to no dot, in utero 3D information procurement regularly takes a few hours [2] to obtain, which makes in vivo high-throughput imaging unrealistic. HFU does not give as solid a tissue differentiate as MRI and has dot, yet HFU can get 3D information in a matter of minutes with the possibility to give continuous, dynamic.

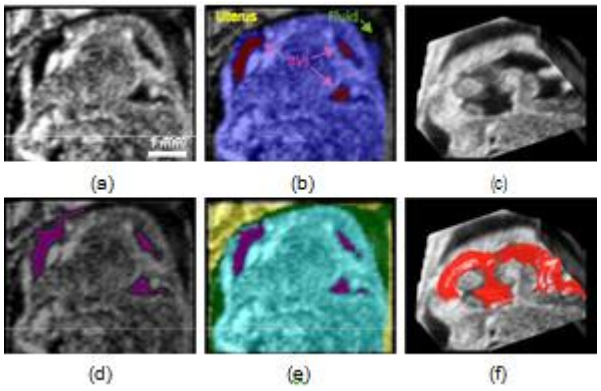

Figure 1. (an) A mid-sagittal area from a 3D ultrasound dataset of a mouse fetus (head district as it were). (b) Manual division of (a). The red locales are BVs, the blue is the head, the grayscale area outside the head is the uterus, and the low-force part between the head and the uterus is amniotic liquid. (d) Region developing to portion the ventricle district beginning from some underlying seeds yields an outcome that holes past the missing limit of the head. This outcome was acquired when the separation of the developed pixel to the underlying seeds was

compelled to be beneath a specific limit. Without such an imperative, there would have been more spillage. (e) The proposed technique can effectively section this picture into four sections: the ventricle (maroon), the head (cyan), the amniotic liquid (green), and the uterus (yellow). Since the ventricle is compelled to be inside in the head, it can't spill out. (c)(f) The 3D rendering of the first volume and the BVs division result.

data [3]. Because of its quick 3D information securing capacity and the accessibility of business and research ultrasound scanners that are generally cheap contrasted with MRI, HFU has turned into a promising device for fast phenotyping of mouse developing lives [3].

With the capacity to gain broad measures of 3D information, robotized or semi-mechanized strategies to examine morphology or organ work are exceedingly attractive. Such investigations expect division to appropriately break down and describe the distinctive structures inside the creating incipient organism. For instance, accu-rate division of the cerebrum ventricles (BVs) and head is basic for evaluating the typical and unusual advancement of the focal sensory system of mouse developing lives [3]. Ordinarily, these structures are physically divided, making examination of phenotype exceptionally tedious. A computerized calculation would allow quick and effective fetus organizing and discovery of mind phenotypes, and would make it more productive to perform considers with expansive incipient organism checks.

A HFU picture of the leader of a mouse incipient organism acquired utilizing a 40-MHz, five-component, annular-cluster framework [3][4] is appeared in Figure 1(a). The BVs and the amniotic liquid situated between the head and the uterus each have low force. Because of the nearness of the BVs to the edge of the head, lost ultrasound motion from specular reflection will prompt lost the head limit and, hence, the BVs and the amniotic liquid locales may seem to get in touch with each other. In this circumstance, regardless of whether the underlying seeds were picked inside the BVs, the last sectioned BVs found with strategies that rely upon force data, for example, area developing [5], may spill out of the head, as appeared in Figure 1(d). Albeit some division strategies, for example, dynamic shape (snakes) [6], can utilize smoothness imperatives to counteract spillage, a great introduction is fundamental. What's more, smoothness requirements in snakes can't manage expansive missing limits between the head and the uterus. One approach to section objects with missing limits is to make utilization of shape models, for example, the dynamic shape demonstrate (ASM) got from physically divided information [7]. Be that as it may, ASM requires a thick arrangement of highlight focuses to properly show the subtle elements of complex shapes. In our earlier work, we built up a half and half technique that joined ASM and shape-compelled district developing to diminish the quantity of highlight focuses [8]. Nonetheless, to catch the shape varieties between various datasets, an extensive number of physically fragmented datasets are important to create an adequate number of eigen-shapes. Practically speaking, such manual division may not be achievable.

Rather than utilizing particular shape models, fuse of basic imperatives into picture division calculations has picked up consideration as of late. A few strategies speak to the auxiliary earlier between objects by a tree structure, where the leaves speak to the items and branch hubs speak to gatherings, and endeavor the tree structure while deciding the segmen-tation arrangement [9] or illuminating a various leveled cost [10]. There have been a few earlier examinations on utilizing diagram slices [11] to seg-ment numerous items with basic imperatives. Ishikawa [12] proposed to speak to different protests by stacked, isolated layers of a chart with directly requested marks for progressive layers. On the off chance that a regularization term is curved regarding a directly

requested name set, this multi-protest division issue can be understood as a paired diagram cut issue. In Ishikawa's model, the closer view in an upper layer is limited to be a subset of the forefront in the layer beneath by utilizing coordinated between layer edges with an unbounded cost. In spite of the fact that the creator did not talk about how to consolidate basic requirements with this layer-cake structure, Ishikawa's model has been generally utilized as a part of portioning objects with repeating "regulation" relationship. Since the regularization cost of Ishikawa's model isn't irregularity protecting, which implies that the cost between two pixels increments with the distinction of their marks, Ishikawa's model can't authorize a "prohibition" relationship on a par with the Potts demonstrate [13]. Delong and Boykov [14] proposed to make utilization of the known non specific connections between various protests, for example, "control," "fascination," and "rejection." Delong and Boykov's model additionally utilizes an arrangement of layers to speak to all items as in Ishikawa's model, yet every one of these layers are unordered and associated by between layer edges as indicated by basic connections. The known basic limitations are implemented by allotting appropriate expenses along these coordinated between layer edges. Delong and Boykov's model can authorize a control relationship as the Ishikawa's model and uphold an avoidance relationship as the Potts display, however there exists some limitation for the blend of connections. Utilizing an indistinguishable structure from [14], Ulen' et al. [15] proposed to utilize Lagrangian duality to enhance the calculation time and memory use of [14]. Be that as it may, both [14] and [15] are settled in the discrete area and subsequently tend to show a network inclination (metrication mistake) [16].

Late works have concentrated on taking care of multi-protest segmen-tation issues with basic data in the nonstop space (i.e., a pixel is doled out an incentive in the vicinity of 0 and 1, as opposed to 0 or 1). Nosrati et el. [17] proposed a persistent partner of Delong and Boykov's model. This level-set-based approach has a few favorable circumstances, for example, less memory utilization, speedier runtime, and no framework ancient rarities, however it might merge to a nearby rather than a worldwide arrangement. To get a consistent and worldwide ideal arrangement, Yuan et al. proposed a persistent max-stream [18] to fragment various disjoint items (avoidance) by unraveling the raised loose consistent Potts demonstrate [19]. Rajchl et al. [20] stretched out the consistent Potts model to fuse a restricted various leveled requirement, called halfway requested Potts show (POP), for myocardial scar division. In crafted by [20], closer view objects were urged to be near each other by a limit length cost for the forefront. To handle spatially-repeating objects, Rajchl et al. [21] expanded the ceaseless max-stream technique [18] to understand the constant variant of Ishikawa's model. As of late, Baxter et al. [22] broadened this constant max-stream system to fragment objects with a more broad progressive structure like an established tree, in which objects are not by any stretch of the imagination disjoint (as in the Potts display) or are subsets of each other (as in the Ishikawa's model). Baxter et al. [23] additionally proposed a more broad form.

B. Examination of NGC and Delong and Boykov's Model :

To exhibit the benefit of NGC in sectioning pictures with the settled structure, we look at the division aftereffects of two toy illustrations got by NGC and Delong and Boykov's model [14]. Figure 2(a) and 2(h) indicate two settled structures; question 1 is the inward white circle, protest 2 is the dark locale, and the foundation is the white region outside protest 2. In Figure 2(h), there is a missing limit between question 1 and the foundation. NGC can section all territories accurately (Figure 2(i)) when the weight proportion fulfills the lower and upper limits. At the point when the weight proportion is outside these limits, it might prompt an undesired division, as exhibited in Figure 2(j) and 2(k). Note that these

weights essentially rely upon the extent of the missing limit along the aggregate limit of the relating inward area, and are invariant to the scale, course, or introduction of target objects. Once fitting weights are resolved in view of a couple of preparing pictures, they can be reused for different pictures with comparative missing limit extents. For the division of mouse-fetus pictures, all pictures of a similar growth stage can be fragmented effectively with a similar arrangement of weights.

Rather than utilizing parameters, Delong and Boykov's model [14] expects seeds to separate protest 1 and the back-ground. Figure 2(d) and 2(k) demonstrates the consequence of Delong and Boykov's model without seeds. At the point when constrained starting seeds are decided for protest 1 and the foundation, as appeared in Figure 2(e) and 2(l), Delong and Boykov's model can just yield revise division when a limit exists. With adequate starting seeds, the Delong and Boykov's model can yield the right outcome (Figure 2(i)) regardless of whether the limit is mostly missing. Contrasted with strategies utilizing an arched vitality utilitarian, techniques utilizing a non-curved vitality practical (i.e., requiring instatement) can be more precise and more adaptable to accomplish tasteful outcomes. In any case, instatements (e.g., introductory seeds) are not reusable, and it is lumbering and tedious to instate protests physically in a 3D picture. Interestingly, parameters utilized as a part of an arched utilitarian can be prepared utilizing average pictures in every application setting, which are then material to all pictures in a similar setting.

II. METHODS AND MATERIAL [Page Layout]

Settled GRAPH CUT

In this paper, the settled structure alludes to an arrangement of items fulfilling a recursive control relationship. Rather than characterizing the settled connection between objects straightforwardly, we characterize the settled relationship as far as districts, where locale I is the association of articles 1 to I, meant by I, I = 1...L. The settling relationship implies:

1 ✓ 2 • ✓ L ✓

where is the whole picture area. With this documentation, protest

I is equivalent to i\ i–1.

Notwithstanding the previously mentioned subset limitations, when a few items are not shut (e.g., the open ring in Figure 2(h)), NGC additionally requires that I be inside the arched structure of i+1. This necessity is utilized to characterize the missing bound-ary between two reaching objects having comparable force disseminations (Figure 2(i)). NGC does not require seeds from clients to separate articles with comparable power and makes all voxels inside the curved structure of question I + 1 be conceivable possibility for protest I. For instance, in Figure 2(h), there are two white regions inside the raised body of question 2 (dark zone) which are contender for protest 1, as appeared in Figure 2(j). For this situation, NGC can get three distinctive division comes about (Figures 2(i) to 2(k)). Clients can acquire the coveted NGC division come about by setting weighting parameters in the vitality useful (1) legitimately. In this work, we likewise infer the vital conditions to get the coveted division result, as in Figure 2(i).

This segment is sorted out as takes after: Sec. II-A depicts the structure of settled chart (NG) and characterizes all the vitality terms utilized as a part of NG. Sec. II-B acquaints and talks about how with dole out weights in the vitality capacity to control the aftereffect of NGC. Sec. II-C clarifies the significance of the cushioned pixels in NG.

A. Nested Graph and Its Energy Function

1) Graph structure: To authorize the settled structure, both Ishikawa's model [12] and Delong and Boykov's model [14] stack all diagram layers in a settling request and utilize guided edges to associate neighboring layers. The proposed NG moreover takes

after this general structure. Figure 3 delineates the NG of two settled protests over a foundation appeared in Figure 2. Like Ishikawa's model, each layer in NG has connects just with its upper and lower neighboring layers. Since the division aftereffect of a settled structure basically fulfills the subset imperative, NGC does not have to utilize coordinated between layer edges as in Ishikawa's model. All the more by and large, for a structure with L settled articles, the NG will have L layers with the best layer speaking to the deepest protest. In NG, just the best layer has connections to the sink T (associating with it implies the pixel is thought about foundation in this layer), and just the base layer has connections to the source S (interfacing to it implies the pixel is thought about forefront in this layer). Since for any pixel just a single between layer edge will be cut when fathoming the NGC, regardless of how this multi-layer chart is cut, the subsequent districts will dependably fulfill the predescribed settling relationship. For instance, if the edge between layer I – 1 and layer I is cut, this pixel is associated with the sink at layers 1 to I – 1 (i.e., it is considered foundation in layers 1 to I – 1), and is associated with the source at layers I to L (i.e., it is thought about frontal area in layers I to L or are in locales I to L). This implies this pixel is divided to have a place with protest I.

2) Energy Functional and Edge Costs: We utilize variable xip to show the division result, with xpi = 1 indicating Fig. 3: The NG for fragmenting a picture containing two settled questions over pixel p is alloted to locale I and xpi = 0 showing pixel p is a foundation (e.g. Figures 2(a) and 2(h)). S and T mean the source and the not in area I. Give P a chance to mean the arrangement of pixels and N the neigh-sink, separately. Wp is the vitality cost of between layer edges. The closer view (hubs associated with source S) in layer 1 (top layer) speaks to locale 1, which borhood structure characterizing the arrangement of associated pixel pairs refers to the inward white circle. The frontal area in layer 2 (base layer) in the whole picture. In our investigations for portioning 3D represents locale 2, which is the dark territory outside area 1 or more protest 1. pictures, we utilized 18-network to characterize the neighborhood The dark hubs in each layer speak to pixels in the info picture and the hued hubs are cushioned limit hubs structure. Following the first diagram cuts detailing [31] to decide xpi, we limit the accompanying vitality utilitarian:

$$E(x_p^i, i = 1..L, p\ 2\ P) = \sum_{i=1}^{L}\sum_{p2P} D_p^i(x_p^{i-1}, x_p^i) + \lambda_i \sum_{pq2N} V_{pq}^i(x_p^i, x_q^i)$$

$$D^i(x^{i-1}, x^i) = \begin{cases} 0 & x^i \\ P & p\ p\ P\ (\ -\log(W_p^{i-1,i}) \\ & x_p^i \end{cases}$$

$$\begin{cases} 1 & > \dfrac{I_p - I^T}{\quad} \quad \text{region i has low intensity} \\ & \quad 1, \\ i & 8\ 1 + \exp(\ \sigma\ ) \\ I & \\ (I_p) = > & p\ I^T \\ > & \exp(\ -\ ) \\ > & \sigma \\ > & \dfrac{\quad}{\quad} \quad \text{Otherwi} \\ < & T\ , \quad \text{se} \\ > & \\ & Ip-\sigma \\ > & 1 + \exp(I\ \ ) \\ > & \\ : & \end{cases}$$

$$V_{pq}(x_p, x_q) = \begin{cases} i\ i\ i & 0 \quad x_p^i = x_q^i \\ (1 & x_p^i = x_q^i \end{cases}$$

6

Following the ordinary documentation of chart cut strategies,

Dpi and Vpqi in Eq. (1) remain for the information term and the regularization term, separately. Note that we characterize the information cost in Eq. (2), so that if a pixel is as of now alloted to protest I with a cost contingent upon its power, this pixel won't cost extra vitality in every single other layer.

In this paper, since we apply our technique to HFU pictures of mouse developing lives, we just think about the situation where each protest has either high or low force. As showed in Figure 1, the force of BVs is "low," the power of the head is "high," the force of the amniotic liquid is "low," and the force of the uterus is "high." Ideally, the term Wpi,i–1(Ip) ought to be the restrictive likelihood that power Ip has a place to district I. We inexact this restrictive likelihood by a sigmoidal capacity characterized in Eq. (3). The paramters IT and σ are resolved naturally in light of the watched force shaded hubs are cushioned limit hubs circulation of the picture. The points of interest are depicted in SecIII-B.

In traditional chart cut techniques, the edge cost Vpqi is ordinarily contrarily relative to the spatial slope between pixels p and q, so the cut occurs on the edges with a high inclination. Such a definition, notwithstanding, won't function admirably in pictures with missing limits since it will debilitate cutting along the missing limit. Rather, we characterize each V I as in Eq. (4), so limiting the edge cost in each layer pq, I is comparable to limiting the cut length. By limiting this length, NGC favors smooth locale limits.

B. The Ratio of ↵i /↵ i+1
i i+1

The coefficient ↵I in the vitality practical (1) is utilized to measure the limit cost of the distinguished area I. By and large, the coefficient ought to be adequately substantial to advance smooth protest limits yet not very huge to maintain a strategic distance from the converging of diverse items as a result of oversmoothing. At the point when all articles in the settled structure have unmistakable force circulations, each layer can have subjective weight as expressed in Delong and Boykov's model. In our examination, we force limitations on the coefficient proportions ↵i/↵i+1 to advance right division at the point when a few articles have comparable force conveyances. Specif-ically, when question I and protest I + 2 have comparable power disseminations, we utilize the arched body of a halfway question (question I + 1) as a shape imperative to characterize the limits between question I and protest i+2, and the quality of the shape imperative from question i+1 can be controlled by the coefficient proportion ↵i/↵i+1.

NGC treats all parts inside the curved body of protest I + 1 as contender for protest I. Addendum An infers the upper bound and the lower headed for the coefficient proportion ↵i/↵i+1 to get attractive outcomes. In Figure 2(h), there are two internal segments inside the arched structure of the dark question (protest)

2) as appeared in Figure 2(j). Fundamentally, the upper bound is forced with the goal that the bigger green locale in Figure 2(j) can be isolated from the external yellow locale regardless of the missing the limit between the two.The upper bound is constantly less than or equivalent to 1, which implies that ↵i < ↵i +1. This is vital with the goal that the green district and the yellow area will not be dishonestly converged into a similar locale (as in Figures 2(d) and 2(k)). At the point when part of the limit of area I is feeling the loss of, the upper bound relies upon the limit missing rate of locale I (see Appendix A for formal definition). The lower bound is forced with the goal that the little green area in Figure 2(j) won't be dishonestly considered to have a place with an indistinguishable locale from the bigger green district. The little green area is the distinction between the arched frame of the dark district and the dark locale. This area exists in light of the fact that the external limit of the dark district is non-arched. The lower bound is 0 if the

limit is raised. By and large, the lower bound relies upon the limit convexity rate of area I + 1, formally characterized in Appendix A. Note that these limits are not touchy to the variety between various pictures; thusly, a similar arrangement of coefficients is utilized to section all pictures in the same gestational stage. As appeared in Figure 2, when the coefficients are fulfilled these limits, one can get right division comes about even within the sight of missing limits and non-raised limits.

C. Cushioned Nodes along the Image Boundary

One critical distinction between our chart and Ishikawa's or Delong and Boykov's diagram is that we include cushioned hubs along the picture limit. Without such cushioned hubs, NGC may acquire false division, as appeared in Figures 2(g) and 2(n). In this outcome, the whole white territory in the first picture is sectioned as district 1 in layer 1, with a cut length of S1 + S2, and the whole picture as locale 2 in layer 2. This outcome fulfills the control limitation and its regularization term is ↲1(S1+S2). Then again, for the right division result in Figure 2(b), the cut length in layer 1 is S1 and that in layer 2 is S2, and the aggregate regularization cost is ↲1S1 + ↲2S2. Review that the upper headed for the alpha proportion requires that ↲1 < ↲2, so the regularization cost for the wrong division in Figure 2(g) is littler than that for the right division in Figure 2(b). Note this false division is caused by not relegating any cost when the cut between the frontal area and the foundation is along the picture limit.

To stay away from this issue, each layer in NG is cushioned with a one-pixel-thick limit around the picture area (outlined by the red and green focuses in Figure 3). We compel these cushioned hubs to be associated with the sink (consequently considered foundation pixels) by allotting an endless cost on the connection interfacing with the sink and zero cost on the connection associating with the source (orange undirected connections in Figure 3). A comparative setting has been utilized as a part of [27]. With these cushioned hubs, the cut length in layer 2 for the outcome in Figure 2(g) progresses toward becoming S3, prompting an aggregate regularization cost ↲1(S1 +S2 +S3) +↲2S3. Then again, the aggregate regularization cost of the right divisions in Figure 2(b) stays at ↲1S1 + ↲2S2, littler than the cost of the false division in Figure 2(g) with appropriate proportion ↲1/↲2.

III. GENERAL FRAMEWORK

Figure 4 shows the entire system of our calculation. The info picture is pre-handled to de-clamor and increment differentiate, at that point the edge work is acquired and multi-determination NGC is connected to spare calculation time, lastly, the outcomes are present prepared on revise clear seg-mentation mistakes. The subtle elements of all means are portrayed underneath.

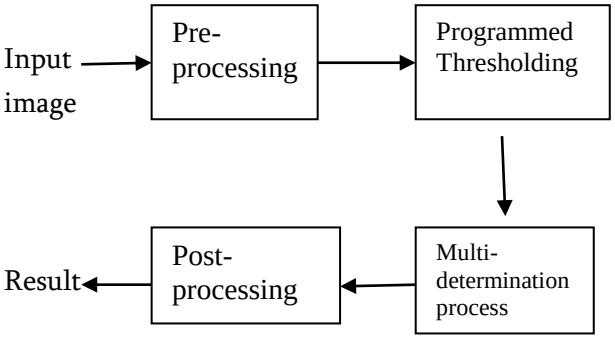

Figure 4. The flowchart of proposed segmentation framework. The corresponding results are illustrated in Figure 7.

A. Pre-processing:

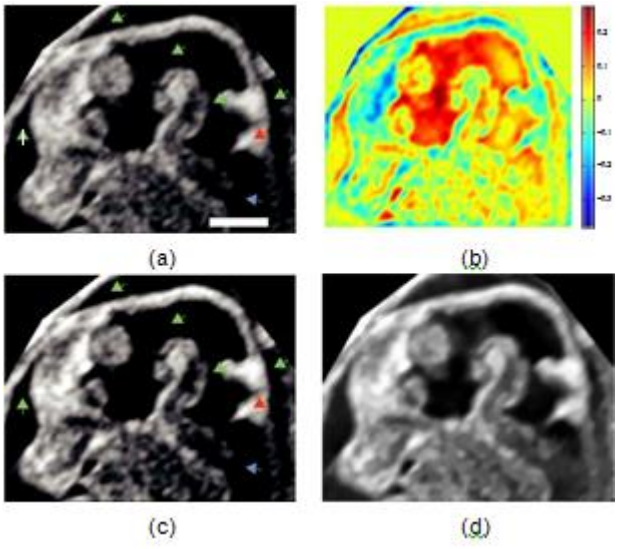

Fig.ure 5. (a) The original ultrasound image f. Scale bar = 1mm. (b) The compensation term g obtained by two low-pass filters. Positive values at narrow gaps and negative values at tissue edges can increase the contrast between different objects. (c) The pre-processed image f^0 obtained by deducting the compensation term from the original image. (d) The result after applying the coherence filter.

In the mouse-foetus HFU pictures (e.g., Figure 5(a)), because of high-power clamor, a few pixels (green bolts) in BVs and amniotic liquid may have more noteworthy force than the force of a few pixels of the head (the blue bolt). This sort of commotion has a tendency to occur along the tight hole between solid edges, for example, the head and the uterus and the limited piece of the BVs. To alleviate comparative clamor, known as the corona relic in fluorescence pictures, the versatile area based appropriation work (ARBD) [32] was proposed. In our examination, we changed ARBD to pre-process the 3D HFU pictures and get a "pay" picture (Figure 5(b)). This picture has high esteems at the thin hole amongst edges and low (even negative) values at the edge of tissue. We at that point achieve the pre-handled picture f 0 by subtracting the pay term g from the first picture f:

$f^0 = f - \gamma g$

where $g = (f \nleftarrow h) - (f \nleftarrow p)$

The pay term, g (Figure 5(b)), is the distinction between the convolution consequence of two Gaussian channels h and p. By deducting the remuneration term, the high-force commotion at the thin hole is dispensed with, and the differentiation of the edge is expanded (Figure 5(c)). Furthermore, following the utilization of ARBD, we additionally apply a soundness channel as depicted in [33] to f0 to smooth the picture and upgrade the edges (Figure 5(d)).

B. Programmed Thresholding

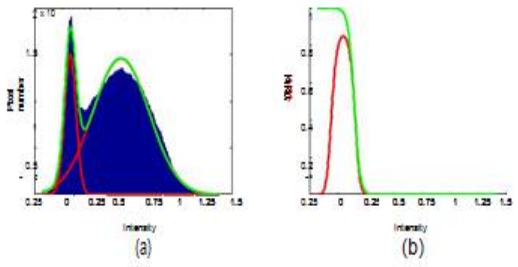

Figure 6. (a) The blue area shows the histogram of the processed image in Figure 5(d). Gaussian mixture model (red lines) is used to fit the histogram to represent the distributions of the low-intensity region and the high-intensity region. Green line shows the sum of Gaussian mixture model. (b) The red curve represents the conditional probability of the low-intensity region estimated based on the GMM model. The green curve is the corrected estimate, by fitting a sigmoid function to the right edge of the red curve.

To decide the parameters in the sigmoid capacity utilized as a part of Eq. (3) consequently, we right off the bat fit a Gaussian blend demonstrate (GMM) with two blends to the histogram of the pre-handled picture by the delicate Expectation Maximization (EM) calculation [34]. Since the EM calculation tends to achieve a neighborhood optima, we instate the EM calculation by isolating all pixels into two gatherings with a few limit esteems and pick the fitted outcome with the littlest mean square mistake. Figure 6(a) demonstrates the best fitted outcome for an illustration picture. After we get GMM parameters, we can compute the contingent likelihood of a power esteem I has a place with a specific area R. The red bend in Figure 6(b) demonstrates the contingent likelihood for the low-force area decided from the evaluated GMM parameters. Note this evaluated condi-tional likelihood is off base at the low-power locale. Rather than utilizing this likelihood as may be, we fit a sigmoid capacity (green bend) to the correct side of red bend and utilized it to decide the information term in Eq. (3). The edge IT is set as the crossing point of two Gaussian conveyances

(weighted by their person earlier probabilities), and the parameter σ is resolved from the slant of the red bend in the vicinity of 80% and 20% of the pinnacle esteem separating by –0.2181, which is the incline of the sigmoid capacity in the vicinity of 0.8 and 0.2 when σ=1.

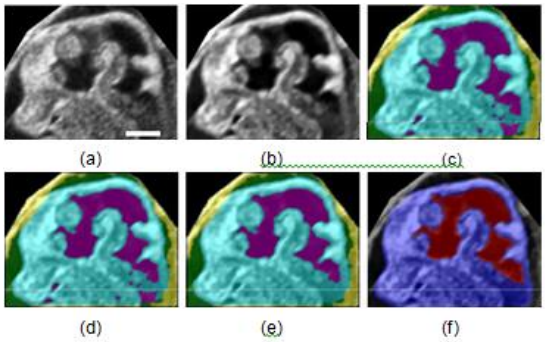

Fig. 7: Intermediate results of all steps in Figure 4. Scale bar = 1mm. (a) Target HFU image. (b) The image after pre-processing. (c) The segmentation by NGC at low resolution. (d) Refined segmentation by NGC at full resolution. (e) The result after post-processing. (f) Manual segmentation result.

Figure 7

In our execution, we initially standardize the first inten-sity esteems to the scope of 0 to 1. After pre-preparing, some pixles have values outside this range. We apply dissemination estimation specifically on the handled information to decide the parameters for the sigmoid capacity. Be that as it may, we truncate the handled esteems to the scope of 0 to 1 preceding applying NGC to the pre-prepared picture.

C. Multi-determination Process

In our trial, we connected a discrete max-stream calculation proposed in [35] to cut the NG. The multifaceted nature of the calculation is O(mn2|C|), where m is the quantity of edges, n is the quantity of hubs, and |C| is the length of a cut. In NGC, the quantity of hubs n = LN, where L is the quantity of articles and N is the quantity of voxels. At the point when the quantity of hubs is extensive, the calculation time of this technique increments significantly. To lessen the calculation time, we separate the whole division errand into two stages. The low-determination stage introduces all areas, and the refine stage yields the last division aftereffect of every district. In the low-determination stage, we apply 3-layer NGC to the low-determination picture, which is acquired by downsampling the first picture by a factor of 2 in each measurement. As appeared in Figure 7(c), after the low-determination process, we ordinarily get a division result where the limits of all items are near the ideal position. In the refine stage, the limit of all items can be refined by 2-layer NGC at the full determination dynamically. Since all articles have a settling relationship, the limit of protest I is just limited by question i+1 and question i+2. In this manner, we can utilize a 2-layer NGC on the pixels that are in the association of articles I to I + 2 from the low-determination answer for refine question I. For every 2-layer NGC, all pixels at first named other than I to I + 2 are settled with the goal that it requires considerably less investment than running full-determination NGC over all items at the same time. Figure 7(d) demonstrates the aftereffect of NGC subsequent to refining all areas.

D. Post-preparing

The BV framework is a ceaseless liquid filled cavity with four morphologically unmistakable parts: two horizontal ventricles in addition to the third and fourth ventricle (Figure 8(e)). For fetuses at E12.5 and more seasoned, these four ventricles are associated by limit between ventricular trenches. These limited waterways may not be noticeable in HFU pictures, and the measure of separated BV parts differs from 1 to 4. Despite the fact that an appropriate coefficient proportion ↲i/↲i+1 can enable NGC to dispense with segments caused by a non-raised limit as depicted in Sec. II-B, NGC may even now yield some undesirable segments inside the head as BVs as appeared in Figure 7(d). To expel the mistaken piece of the BVs naturally, we incorporated a post-handling venture to the consequence of NGC. Initial, an associated part examination of the underlying aftereffect of BVs is performed, and these segments were arranged by diminishing volume. Clearly, the biggest segment must be a piece of the BVs, and is utilized to start the BVs in the accompanying iterative process. Iteratively, the volume of the following biggest associated part is contrasted with the volume of the current BVs. In the

event that this volume is bigger than b% of the current BVs, at that point this associated part is added to the current BVs. This iterative procedure is performed until the point that an associated segment neglects to be added to the current BVs. Figure 7(e) demonstrates the outcome after the post-preparing process.

IV. EXPERIMENT SET-UP

A. Image Acquisition

Table 1. Images in 5 gestational stages.

Stage	With manual BVs and head segmentation	With manual BVs segmentation only
E10.5	6	3
E11.5	7	2
E12.5	6	4
E13.5	5	3
E14.5	4	0
Total	28	12

The 3D, HFU, mouse-incipient organism pictures were gained with a 40-MHz, five-component, annular-exhibit framework completely de-veloped at Riverside Research [4], [3], [36]. For this investigation, 40 mouse-incipient organism 3D pictures traversing five mid-gestational stages from E10.5 to E14.5 (Table I) were utilized, where E0.5 was characterized as twelve of the day after fruitful overnight mating. The measurement of the 3D picture increments relying upon gestational stages, running from 111 by 149 by 40 to 200 by 200 by 100 voxels. The voxel size of the 3D HFU datasets was 25 by 25 by 50 μm. The ultrasound framework and imaging conventions are portrayed in incredible detail in [3] and all creatures utilized as a part of these investigations were kept up under conventions affirmed by the Institutional Animal Care and Use Committee at the NYU Langone Medical Center. For each of the 40 pictures, self-loader divisions of BVs were accessible [3], while just 28 out of the 40 pictures had manual divisions of the embryonic head accessible. The shape of the embryonic head was physically drawn utilizing Amira representation programming by a little creature ultrasound imaging master [3]. We utilized these manual divisions as ground truth to evaluate the execution of our calculation.

B. Parameter Selection

Table II compresses the parameter settings utilized as a part of our test. We gather these parameters into two classes. Note that pre-and post-handling are for the most part required for other division strategies also. Contingent upon the picture attributes, other pre-and post-preparing techniques could be utilized. The center NGC calculation for dividing four articles with settled relationship required just three parameters.

Table 1. Parameters used in the proposed segmentation method

Parameter	Description	Eq.	Value
	NGC		
$↵_1/↵_2$	Coefficient ratio of ventricle and head	(1)	0.5
$↵_2/↵_3$	Coefficient ratio of head and amniotic fluid	(1)	0.1 (E10.5, E11.5) 0.33 (other stages)
$↵1$	Weight of the top layer	(1)	10^{-3}
	Preprocessing & Postprocessing		
C	Size of the small low-pass filter p	(5)	3
A	Size of the large low-pass filter h	(5)	9
Γ	Weight of compensation term	(5)	1
B	Threshold of BV volume ratio		10%

There are two stages to decide the coefficients ↵i. The initial step is to decide the ↵i/↵i+1. At the point when

question I and protest I + 2 get in touch with each other, the limit between them might miss if the forces of these two articles are comparative. As appeared in II-B, by setting the proportion ↵i/↵i+1 to be between the lower and upper bound, NGC can isolate protest I and question I + 2 accurately with a limit that is adequately the arched frame of the middle of the road protest I + 1. Subsequent to getting ↵1/↵2 and ↵2/↵3, we can decide all coefficient ↵i by setting coefficient ↵1. Points of interest on the most proficient method to appraise the lower and upper bound and set the proportion ↵i/↵i+1 in view of the attributes of pictures to be sectioned are talked about in Sec. V-D.

As per the determination in Appendix A, the limits of the coefficient proportion ↵i/↵i+1 rely upon the limit missing rate and the limit convexity rate of protest I and question i+1, separately. The limit missing rate of BVs is beneath 1/4 and the limit convexity rate is bigger than 1/4 in view of the perception of our pictures, and subsequently we set ↵1/↵2 as 0.5 in view of Eq. (8) in Appendix A for all pictures. Since the limit missing rate of the head is bigger than the limit missing rate of BVs, the proportion ↵2/↵ 3 is littler than ↵1/↵2. For stages E12.5 to E14.5, we set the proportion to 0.33 to get an acceptable division. For stages E10.5 and E11.5, the limit missing rate of the head is considerably bigger and makes the upper bound littler than 0.33. In this manner, we set ↵2/↵3 as 0.1 in E10.5 and E11.5. The affectability of the calculation execution to the coefficient proportion ↵i/↵i+1 is portrayed in Sec. V-D.

After the proportions ↵i/↵i+1 are chosen, we set an appropriate ↵ 1 to adjust the information term and the regularization term. Note that ↵1 ought to be corresponding to the volume to surface proportion of the protest in layer 1, which is thusly relative to the determination of the picture for a round question. By assessing the consequence of NGC in a couple of cases, ↵1 was picked as 0.001 in full determination in our trial, and ↵1 in the low determination was set to half of this esteem, or 0.0005.

For pre-preparing, the size c of the Gaussian channel p was been the width of the most slender piece of the protest with low power (e.g., hole width between solid edges (green bolts in Figure 5(c)) in the ultrasound picture, and was set to c = 3 in our trial. The size, an, of the Gaussian channel h was three times the extent of p (i.e., a = 3c). The standard deviation of each Gaussian channel is set to be channel estimate isolated by 2 log 2. At long last, γ, the heaviness of the pay term, was set to 1 for all pictures in our analysis.For post-processing,the limit of BV volume proportion was set as b = 10% for all pictures by checking a few consequences of BV division.

C. Reference Methods

We looked at the execution of NGC for the whole dataset to three techniques: ASM, area developing introduced by ASM (ASM+RG), and our past work, which refines the ASM result by shape-obliged district developing (ASM+SCRG) [8]. All these correlation strategies were utilized to portion BVs and the head, and are talked about beneath. We likewise performed division with the Delong and Boykov's model [14] for a couple of pictures with some physically picked seeds.

For ASM execution, we utilized an individual point appropriation display for BVs and the head and divided them independently. To prepare the point dispersion model of BVs or the head, we separated 250 component focuses (for each model) on the surface of the manual division result from each picture. Highlight focuses in various pictures were naturally coordinated by shape setting [37], and after that used to determine the eigen-shapes. In our reproduction, the quantity of eigen-shapes was set to be the same as the quantity of preparing pictures in each gestational stage. Since we had few pictures that can be utilized for preparing, the restricted eigen-shapes are inadequate to introduce all changeability

in the state of BVs. To assess the execution of ASM, we utilized a forget one cross-approval approach.
ASM+RG utilizes ASM comes about as the underlying seeds, and after that distorts the underlying seed district by both developing and pruning, which implies disposing of undesired beginning seeds. ASM+RG can't anticipate spilling out of BVs into the liquid area because of the missing head limit in a few pictures. Along these lines, we set the most extreme developing separation as 20 voxels from the underlying seed locale to evade excessively spillage. Note that RG can work without ASM. We can likewise instate RG by a constrained arrangement of seeds looked over the objective area physically.

ASM+SCRG [8] first applies ASM to get an underlying segmen-tation result, at that point it enrolls the association of all preparation shapes onto the underlying outcome by ASM as indicated by the situation of historic point focuses to get a halfway division. This middle of the road division contains all subtle elements in the preparation shapes. At that point, it twists this middle division utilizing a changed RG technique that is compelled by the underlying shape. Contrasted with ASM, this strategy can unwind the requirements of eigen-shapes and right the mistake caused by the inadequate thickness of historic point focuses. Be that as it may, its precision is restricted by the execution of ASM.

V. RESULTS AND DISCUSSION [Page Style]

We utilized two criteria to assess the similitude of the division result by a calculation with the manual segmen-tation. The Dice comparability coefficient (DSC) is characterized as:

$$DSC = 2|X \setminus Y|/(|X| + |Y|)$$

where X and Y are the consequence of the division calculation and the ground truth, individually. Voxel separate is the mean separation between all voxels on the surface of the division result to the closest voxels on the surface of the manual division, characterized regarding the quantity of voxels. Tables III and IV demonstrate the execution of four distinct strategies in portioning BVs and heads for all pictures in our dataset. For NGC, we give the outcomes acquired utilizing multi-determination handling, and additionally while applying NGC to the full-determination pictures specifically. Figure 8 gives visual correlation of these four strategies with manual division for an agent E12.5 picture.

With the creating focal sensory system (CNS) in the mouse fetus commanded by the BVs and the encompassing tissue at these mid-gestatioanl stages, the state of the BVs and the head are utilized as biomarkers of typical and unusual CNS improvement. In procuring this information, the encompassing additional embryonic highlights, for example, the amniotic liquid and uterus were somewhat imaged. In this paper, we center around assessing the precision of the BVs and the head, and analyze the execution of NGC and reference calculations for sectioning these two locales. Having precise division of the amni-otic liquid and the uterus isn't applicable since 3D volumetric information from the entire conceptus would have been should have been gained. Be that as it may, we indicate division comes about for the amniotic liquid and uterus for a couple of chose pictures in Figure 9 to show the capability of NGC for dividing all locales all the while.

A. Comparison of NGC with Reference Methods

1) ASM: ASM (Figure 8(b)) can keep the spillage, however it has two primary downsides. Initially, ASM may not precisely locate the genuine BV limits in light of the meager arrangement of highlight focuses. In the 3D rendering of Figure 8(b), numerous BV subtle elements are missing on the grounds that the constrained arrangement of highlight indicates was not able catch and appropriately show the complex BV shape. Second, ASM can't section BV limits precisely utilizing a model which was prepared on constrained preparing pictures. This is on the grounds that the aftereffect of ASM is confined to be a straight

mix of the mean shape and eigen-shapes, and the quantity of eigen-shapes is restricted by the quantity of preparing shapes. For instance, in Figure 8(b), the edge of BVs (red lines) is limited by the preparation shapes, so ASM can't get an indistinguishable edge from those appeared in Figures 8(c), 8(e), and 8(f).

In Table III, ASM gives a more strong execution (i.e., bring down standard deviations) than ASM+RG, however its normal execution in BV division is more awful than ASM+RG due to the inadequacy in highlight focuses and preparing pictures. With just 250 component focuses, ASM can't catch all the BV points of interest. Moreover, the state of BVs changes even at the same gestational stage, and such variety can't be displayed well by nine or less eigen-shapes. Contrasted with BV division, the execution of ASM for the head locale is greatly improved in light of the fact that the head shape is easier than the BVs.

2) ASM+RG: In Figure 8(c), ASM+RG can discover BV limits precisely when the complexity is solid, however seg-mented BVs may spill out from the powerless edges (the red bolt in Figure 8(c)). Also, the limit got by ASM+RG may not be smooth since RG does not have a lv 1 mm 3v 4v lv smoothness limitation (take note of the loud limits in the 3D rendering in Figure 8(c)).

Tables 3 and 4 demonstrate that ASM+RG has the biggest standard deviation estimations of DSC and voxel separate. This implies the execution of ASM+RG is less powerful. Despite the fact that ASM+RG can perform great in a few cases, it causes vast blunders when there are missing limits amongst BVs and amniotic liquid.

Table 3. DSC comparison

	ASM	ASM + RG	ASM + SCRG	NGC with multi-resolution	NGC on full-resolution directly
BVs	0.76±0.05				0.86±0.07
E10.5	0.75±0.13	0.87±0.04			0.86±0.05
	0.79±0.06				0.86±0.07
E11.5	0.86±0.08	0.89±0.04			0.87±0.07
	0.76±0.04				0.89±0.01
E12.5	0.82±0.10	0.89±0.03			0.89±0.02
	0.66±0.09				0.85±0.10
E13.5	0.74±0.09	0.81±0.07			0.85±0.10
	0.63±0.04				0.86±0.02
E14.5	0.53±0.14	0.76±0.04			0.86±0.02
Average	0.73±0.08	0.77±0.14			0.87±0.06
Head	0.81±0.09				0.84±0.01
E10.5	0.75±0.06	0.83±0.10			0.84±0.01
	0.89±0.03				0.88±0.03
E11.5	0.84±0.05	0.91±0.03			0.87±0.03
	0.91±0.03				0.91±0.03
E12.5	0.87±0.04	0.92±0.02			0.91±0.03
	0.89±0.02				0.93±0.01
E13.5	0.89±0.05	0.93±0.02			0.93±0.02
	0.89±0.05				0.93±0.01
E14.5	0.90±0.01	0.90±0.05			0.93±0.01
Average	0.88±0.06	0.84±0.07			0.89±0.04

Table 4. Voxel distance comparison

	ASM	ASM + RG	ASM + SCRG	NGC with multi-resolution	NGC on full-resolution directly
BVs	1.57±0.99				0.86±0.74
E10.5	3.70±3.04	0.65±0.30			0.78±0.53
	1.33±0.48				0.91±0.70
E11.5	1.34±0.94	0.59±0.27			0.89±0.62
	1.16±0.20				0.49±0.16
E12.5	1.90±1.46	0.47±0.20			0.49±0.16
	1.73±0.80				0.90±0.63
E13.5	2.40±1.15	0.89±0.56			0.92±0.68
E14.5	2.67±1.01	1.56±0.66			0.71±0.23

		6.95±3.33		0.75±0.30	
Avera	1.56±0.8	2.78±2.5		0.75±0.4	
ge	0	2	0.73±0.48	0.76±0.56	9
Head		2.77±2.32		2.22±1.48	
E10.5		5.42±1.98	3.30±2.83	2.17±1.54	
		2.06±0.86		2.60±0.88	
E11.5		4.92±0.91	2.21±1.15	2.61±0.89	
		2.30±0.92		1.72±0.39	
E12.5		4.85±1.19	2.37±0.69	1.72±0.40	
		3.71±0.69		2.49±0.50	
E13.5		5.50±1.82	2.94±1.02	2.51±0.50	
		5.54±3.50		3.40±0.72	
E14.5		6.53±2.46	6.13±4.89	3.44±0.76	
Avera	3.06±2.0	5.34±1.6		2.43±1.0	
ge	4	3	3.16±2.52	2.43±0.98	2

3) ASM+SCRG: ASM+SCRG can join the shape con-straint from ASM and refine the come about by utilizing force and inclination data. Figure 8(d) shows that ASM+SCRG can discover the BV limits, yet keep spillage from ASM. In any case, in light of the fact that the shape earlier (middle of the road division) depends on the consequence of ASM, the exactness is additionally limited by the achievable execution of ASM. For instance, contrasting the 3D renderings in Figure 8, BVs' points at the correct side (red lines) seem to be comparable in Figure 8(c), 8(e), and 8(f), however the edges in Figure 8(b) and 8(d) are extraordinary. This is on the grounds that the aftereffect of ASM is limited by the preparation shapes, and the consequence of ASM+SCRG is obliged by the consequence of ASM. As appeared in Table III, ASM+SCRG can enhance normal DSC estimations of ASM by around 0.13, yet its execution stays restricted by the execution of ASM.

4) NGC: The NGC calculation can portion each of the four questions in the meantime to avert spillage. Figure 8(e) represents that the calculation can fragment BVs effectively and additionally isolate the head and the uterus precisely. What's more, NGC sections protests mostly in view of force data, with the goal that its precision execution won't experience the ill effects of the impediment of shape requirements. Because of the regularization term in (1), NGC 1 mm likewise gives a smoother division result than ASM+RG. In Tables III and IV, NGC gave the biggest normal DSC and near littlest voxel remove for the division of BVs among all strategies. The normal standard deviations of these two criteria are generally little much of the time. In early gestational stages, the execution of ASM+SCRG is somewhat superior to NGC. Be that as it may, NGC performed much superior to ASM+SCRG in late gestational stages when the shape variety of BVs is extensive. NGC was not affected by the substantial variety fit as a fiddle among various datasets and gestational stages, and it can give exact division with no shape earlier (aside from the settled connection amongst items) and beginning seeds. For the head division, NGC either gives the best exactness or is near the best of alternate strategies. Since the head shape is moderately straightforward, the change of NGC over different techniques was generally little what's more, is near the ASM+SCRG strategy all things considered. NGC with multi-determination yielded almost indistinguishable outcomes as NGC on the full determination straightforwardly. This is not surprisingly in light of the fact that NGC with multi-determination discovers its ideal by refining the aftereffect of NGC at low determination. For a lion's share of test pictures, the outcome acquired with NGC at the low determination is near the outcome got with NGC on full determination straightforward.

B. NGC Performance for Different Gestational Stages

The structure of the BVs changes drastically finished the five gestational stages explored, as confirm in Figure 9. By and by, the same NGC calculation could auto-matically portion the head and the BVs for every single gestational stage. NGC performs division in view of the force data and thus isn't touchy to the shape variety of BVs in various stages. Using the regularization term to implement smoothness along the area limits, NGC basically characterizes the

missing limit between the head and the uterus by the arched body of amniotic liquid locale. In the consequence of NGC appeared in Figure 9(c), the limit of the upper left piece of the head (red bolt) is straight on the grounds that the arched frame associated amniotic liquid districts (dull green) by a straight line with insignificant separation. All in all, the limit of the head might be erroneously characterized when the genuine head area isn't secured by the curved structure of amniotic liquid areas.

C. Correlation with the Delong and Boykov's Model

We subjectively assessed Delong and Boykov's model on model pictures utilizing a similar vitality practical as de-scribed in (1). Figure 10 demonstrates three illustrative division aftereffects of Delong and Boykov's model on an E12.5 incipient organism picture. We added similar coefficients ↲i to weight the regularization term of Delong and Boykov's model as the setting of NGC in Figure 11(b). With no underlying seeds, De-long and Boykov's model can't separate BVs from amniotic liquid (Figure 10(a)). With restricted seeds for all questions, a few parts of BVs and amniotic liquid can be separated appropriately (Figure 10(b)), yet numerous wrong areas remain (e.g., the limit between the head and the uterus on the correct side). At long last, with adequate seeds for amniotic liquid and the uterus, the division result (Figure 10(c)) is like the outcome acquired by NGC (Figure 11(b)) despite the fact that there are still a few pixels in the liquid district that are mislabeled as BVs.

D. Affectability of NGC to ↲i/↲i+1

We utilized one E12.5 picture to explore the affectability of the NGC calculation to the estimations of the ↲ proportion. Figures 11(a) to 11(c) are division comes about acquired with chose blends of ↲1/↲ 2 and ↲2/↲3. Figures 12(a) and 12(b) analyze DSC esteems for the BV and head, individually, acquired with 11 by 11 distinct blends of ↲1/↲2 and ↲2/↲3. All outcomes were gotten by 3-layer NGC at low determination and were present handled on evacuate wrong BV segments (as depicted in Sec. III-D). By inspecting the manual division consequence of this specific case (see Figure 7(b) for one cut), the limit missing rate between objects 1 (BVs) and 3 (liquid) is 0, and that between objects 2 (head) and 4 (uterus) is 0.19. Hence, the upper bound of ↲1/↲2 is 1 and the upper bound of ↲2/↲3 is 0.62. The lower bound is more hard to decide on the grounds that it relies upon the limit convexity rate, which is difficult to evaluate. Figures 12(a) and 12(b) exhibit that the division precision for the BV and head essentially drops when ↲1/↲2 and ↲2/↲3 dip under 0.2 and 0.1, separately, recommending that these are the lower limits. As appeared in Figures 12(a) and 12(b), as long as the coefficient proportion is between the lower and upper limits, agreeable divisions can be acquired.

In the testing information we have, the limit missing rates of BVs and the head did not shift drastically in various pictures. We could accomplish precise division with a similar arrangement of coefficient proportions for each gestational stage. By and by, we can without much of a stretch decide upper limits by assessing the conceivable scope of limit missing rate. The lower limits are more hard to decide as it is harder to gauge the limit convexity rates of the picture to be divided. Rather than attempting to decide the lower bound, one can simply set ↲i/↲i+1 a smidgen lower than the upper bound, and if the division result isn't attractive, one can marginally expand the proportion if NGC portions undesirable parts into protest I (e.g., the pink district around the nose in Figure 11(a)), and lessen the proportion somewhat if question I is converged into question I + 2 (Figure 11(c)).

E. Complexity Analysis

Table 5. Run time (seconds)

ASM + RG	ASM	ASM + SCRG	NGC with multi-resolutio	NGC on full resolutio

			n	directly
E10.	36.92±1.11	57.37±6.	239.9±21	340.0±23
5	36.06±1.10	05	0.0	0.1
E11.	38.08±0.59	109.4±2	514.8±21	1238±83
5	36.33±0.27	7.7	3.5	4.4
E12.	39.19±0.35	132.7±1	1143±56	1884±93
5	36.81±0.16	6.2	8.6	9.9
E13.	42.54±1.21	254.5±4	1750±11	2880±18
5	38.13±0.44	7.1	82	20
E14.	44.68±2.31	306.1±10	2132±12	4084±25
5	38.93±0.87	2.7	60	34
Avera	39.81±2.93	157.3±9	959.4±90	1723±16
ge	37.07±1.20	7.6	3.3	25

We actualized the NGC strategy utilizing MATLAB 2013a and called a C-usage of the maximum stream calculation [35] for limiting the vitality practical in Eq. (1). Table V records the aggregate calculation time in seconds of five strategies in sectioning BVs and the head area by a PC with a 2.6-GHz i7 processor. Since the chart measure increments with the span of the incipient organism, the calculation time increments with the gestational stage, particularly for NGC.

Of course, NGC with multi-determination NGC is significantly speedier than NGC on full determination. Contrasted with NGC, the calculation time of ASM does not change much at various stages in light of the fact that the point appropriation models all had the same number of focuses. By and by, NGC run time is longer than every other strategy. In any case, it ought to be noticed that NGC does not require tedious client associations to introductory seeds or to create preparing pictures that are required for ASM.

VI. CONCLUSION

In this paper, we presented a novel, completely programmed NGC technique to fragment a picture (2D or 3D) with settled articles. We described how to build the diagram and set the information term and regularization term in the vitality cost to authorize the settled connection between objects. We additionally inferred the conditions that the weighting coefficients in the vitality cost must need to fulfill to acquire an acceptable division within the sight of missing limits when non-contiguous articles have comparative powers. The strategy just makes utilization of the general auxiliary information about the settled connection between the items and does not require any shape earlier (got from preparing information) or physically picked seeds. The technique was connected to 3D HFU pictures of mouse incipient organisms to at the same time section BVs and the embryonic head. It accomplished high exactness on an aggregate of 40 3D pictures in five diverse gestational stages (10.5 days to 14.5 days of development). Thusly, NGC could turn into a precious device to streamline mind development examines utilizing mouse incipient organisms right now requiring tedious manual division.

In spite of the fact that we just analyzed the utilization of the NGC technique for the division of the mouse-incipient organism pictures, it is for the most part relevant to the division of other im-ages containing settled items. The proposed strategy is likewise appropriate to different pictures containing settled items where diverse articles may have in excess of two prevailing hues. For instance, 3D HFU pictures of naturally extracted human lymph hubs (LNs) gained from colorectal-growth patients, contain three settled parts, LN-parenchyma (LNP), fat, and phosphate-cradled saline (PBS) [38]. In a different report [39], we have connected NGC for the division of such LN pictures and demonstrate that NGC can accomplish exact division notwithstanding when there are missing limits amongst LNP and PBS caused by diffraction and acoustic lessening.

In our test, we connected a discrete max-stream calculation proposed in [35]. This calculation can give a worldwide ideal arrangement by looking at all conceivable ways from source to sink. Nonetheless, it

will create metrication ancient rarities, and the calculation time of this calculation increments significantly with the picture measure. Since NGC has a comparable layered structure to Ishikawa's model, it is conceivable to change the constant max-stream answer for Ishikawa's model portrayed in [21] to explain NGC, considering that we utilize undirected connections amongst layers and include cushioned pixels around the picture limit. It is likewise conceivable to expand the arched definition of regulation portrayed in [27] with very much characterized locale subordinate coeffi-cients ↵i. Such augmentations will yield computationally more productive arrangements and can stay away from the metrication curios.

NGC accept that every pixel has a place with one of the articles in the settled structure. On the off chance that a picture contains a few districts that don't have a place with the settled objects of intrigue and these areas have a comparable force dispersion as specific protests inside the settled structure, NGC may dishonestly mark these districts. Step by step instructions to effectively distinguish such districts is a testing future research subject. Moreover, the NGC strategy displayed in this paper does not refresh the force circulations of target questions progressively like level-set-based strategies; rather, it evaluates the worldwide conveyances of various items in view of the worldwide power dispersion of the picture in a pre-preparing stage. Later on, we will endeavor to enhance the structure of NGC to make it ready to accurately distinguish non-settled confined protests and handle neighborhood changes in force disseminations.

VII. AFFIRMATION:

The examination depicted in this article was upheld to some degree by the Riverside Research Internship Program.

VIII. REFERENCES

[1]. R. M. Henkelman, "Frameworks science through mouse imaging focuses: encounter and new headings," Annual audit of biomedical architect ing, vol. 12, pp. 143-166, 2010.

[2]. P. Parasoglou, C. A. Berrios-Otero, B. J. Nieman, and D. H. Turn-bull, "High-determination x-ray of beginning time mouse incipient organisms," NMR in Biomedicine, vol. 26, no. 2, pp. 224-231, 2013.

[3]. O. Aristizabal,' J. Mamou, J. A. Ketterling, and D. H. Turnbull, "High- throughput, high-recurrence 3-D ultrasound for in utero examination of em- bryonic mouse mental health," Ultrasound in Medicine and Biology,

[4]. J. Mamou, O. Aristizabal,' R. H. Silverman, J. A. Ketterling, and D. H. Turnbull, "High-recurrence trill ultrasound imaging with an annular exhibit for ophthalmologic and little creature imaging," Ultrasound in pharmaceutical and science, vol. 35, no. 7, pp. 1198-1208, 2009.

[5]. R. C. Gonzalez and R. E. Woods, Digital Image Processing (third Edition). Upper Saddle River, NJ, USA: Prentice-Hall, Inc., 2006.

[6]. M. Kass, A. Witkin, and D. Terzopoulos, "Snakes: Active form models," International diary of PC vision, vol. 1, no. 4, pp. 321-331, 1988.

[7]. T. F. Cootes, C. J. Taylor, D. H. Cooper, and J. Graham, "Dynamic shape models-their preparation and application," Computer vision and picture understanding, vol. 61, no. 1, pp. 38-59, 1995.

[8]. J.- W. Kuo, Y. Wang, O. Aristizabal, J. Ketterling, and J. Mamou, "Programmed mouse incipient organism cerebrum ventricle division from 3D 40-MHz ultrasound information," in Ultrasonics Symposium (IUS), 2013 IEEE International, July 2013, pp. 1781-1784.

[9]. K. M. Pohl, S. Bouix, M. Nakamura, T. Rohlfing, R. W. McCarley, R.Kikinis, W. E. L. Grimson, M. E. Shenton, and W. M. Wells, "A various leveled calculation for mr mind picture parcellation," Medical Imaging, IEEE Transactions on, vol. 26, no. 9, pp. 1201-1212, 2007.

[10]. A. Delong, L. Gorelick, O. Veksler, and Y. Boykov, "Limiting energies with various leveled costs," International diary of PC vision, vol. 100, no. 1, pp. 38-58, 2012.
[11]. D. Greig, B. Porteous, and A. H. Seheult, "Correct most extreme a posteriori estimation for parallel pictures," Journal of the Royal Statistical Society. Arrangement B (Methodological), pp. 271-279, 1989.
[12]. H. Ishikawa, "Correct advancement for markov irregular fields with raised priors," Pattern Analysis and Machine Intelligence, IEEE Transactions on, vol. 25, no. 10, pp. 1333-1336, 2003.
[13]. R. B. Potts, "Some summed up arrange scatter changes," in Math-ematical procedures of the cambridge philosophical society, vol. 48, no. 01. Cambridge Univ Press, 1952, pp. 106-109.
[14]. A. Delong and Y. Boykov, "Comprehensively ideal division of multi-locale objects," in Computer Vision, 2009 IEEE twelfth International Conference on. IEEE, 2009, pp. 285-292.
[15]. J. Ulen,' P. Strandmark, and F. Kahl, "An effective streamlining outline work for multi-district division in light of lagrangian duality," Med-ical Imaging, IEEE Transactions on, vol. 32, no. 2, pp. 178-188, 2013.
[16]. M. Klodt, T. Schoenemann, K. Kolev, M. Schikora, and D. Cremers, "An exploratory examination of discrete and constant shape improvement techniques," in Computer Vision-ECCV 2008. Springer, 2008, pp. 332-345.
[17]. M. Nosrati and G. Hamarneh, "Nearby streamlining based division of spatially-repeating, multi-district objects with part arrangement con-straints," Medical Imaging, IEEE Transactions on, vol. 33, no. 9, pp. 1845-1859, Sept 2014.
[18]. J. Yuan, E. Bae, and X.- C. Tai, "An examination on persistent max-stream and min-cut methodologies," in Computer Vision and Pattern Recognition (CVPR), 2010 IEEE Conference on. IEEE, 2010, pp. 2217-2224.
[19]. J. Yuan, E. Bae, X.- C. Tai, and Y. Boykov, "A consistent max-stream way to deal with potts demonstrate," in Computer Vision-ECCV 2010. Springer, 2010, pp. 379-392.
[20]. M. Rajchl, J. Yuan, J. A. White, E. Ukwatta, J. Stirrat, C. M. Nambakhsh,F.P. Li, and T. M. Diminishes, "Intuitive various leveled stream division of scar tissue from late-upgrade heart mr pictures," Medical Imaging, IEEE Transactions on, vol.